2020

Quantitative estimation of nerve fiber engagement by vagus nerve stimulation using physiological markers

Y. C. Chang

M. Cracchiolo

U. Ahmed

I. Mughrabi

A. Gabalski

See next page for additional authors

Brain Stimulation 13 (2020) 1617–1630

Contents lists available at ScienceDirect

Brain Stimulation

journal homepage: http://www.journals.elsevier.com/brain-stimulation

Quantitative estimation of nerve fiber engagement by vagus nerve stimulation using physiological markers

Yao-Chuan Chang [a, 1], Marina Cracchiolo [a, b, 1], Umair Ahmed [a], Ibrahim Mughrabi [a], Arielle Gabalski [a], Anna Daytz [a], Loren Rieth [a], Lance Becker [a], Timir Datta-Chaudhuri [a], Yousef Al-Abed [a], Theodoros P. Zanos [a], Stavros Zanos [a, *]

[a] Institute of Bioelectronic Medicine, Feinstein Institutes for Medical Research, Manhasset, NY, 11030, USA
[b] The BioRobotics Institute and Department of Excellence in Robotics and AI, Scuola Superiore Sant'Anna, Pisa, 56127, Italy

ARTICLE INFO

Article history:
Received 24 April 2020
Received in revised form
31 July 2020
Accepted 4 September 2020
Available online 18 September 2020

Keywords:
Vagus nerve stimulation
Biomarker
Bioelectronic medicine
Compound nerve action potential
Physiological modeling

ABSTRACT

Background: Cervical vagus nerve stimulation (VNS) is an emerging bioelectronic treatment for brain, metabolic, cardiovascular and immune disorders. Its desired and off-target effects are mediated by different nerve fiber populations and knowledge of their engagement could guide calibration and monitoring of VNS therapies.
Objective: Stimulus-evoked compound action potentials (eCAPs) directly provide fiber engagement information but are currently not feasible in humans. A method to estimate fiber engagement through common, noninvasive physiological readouts could be used in place of eCAP measurements.
Methods: In anesthetized rats, we recorded eCAPs while registering acute physiological response markers to VNS: cervical electromyography (EMG), changes in heart rate (ΔHR) and breathing interval (ΔBI). Quantitative models were established to capture the relationship between A-, B- and C-fiber type activation and those markers, and to quantitatively estimate fiber activation from physiological markers and stimulation parameters.
Results: In bivariate analyses, we found that EMG correlates with A-fiber, ΔHR with B-fiber and ΔBI with C-fiber activation, in agreement with known physiological functions of the vagus. We compiled multivariate models for quantitative estimation of fiber engagement from these markers and stimulation parameters. Finally, we compiled frequency gain models that allow estimation of fiber engagement at a wide range of VNS frequencies. Our models, after calibration in humans, could provide noninvasive estimation of fiber engagement in current and future therapeutic applications of VNS.

Introduction

The vagus nerve innervates most thoracic and abdominal organs and relays afferent and efferent information between peripheral receptors and effector cells and the brain [74]. Cervical vagus nerve stimulation (cVNS) is emerging as a potential treatment for a multitude of disorders affecting the brain and peripheral organs, including drug-resistant epilepsy [2], depression [3], Alzheimer's disease [4], anxiety [5], pain [6], tinnitus [7], rheumatoid arthritis [8], heart failure [9], diabetes [10] and obesity [11], pulmonary hypertension [12,13], and others. The therapeutic actions of cVNS, although still under investigation, are mediated by activation of different types of fibers. For example, anti-epileptic action is thought to be related to afferent, large, myelinated A-fibers [14], cardio-inhibitory action in heart failure to efferent, myelinated B-fibers [15], and anti-inflammatory action by B- and possibly by afferent, unmyelinated C-fibers [16,17]. In addition, some of the off-target effects of cervical VNS that often limit its therapeutic efficacy arise from the activation of large fibers innervating the mucosa and muscles of the larynx and pharynx [18].

To develop safe and effective VNS protocols for existing and future indications, optimization of stimulation parameters with

* Corresponding author.
E-mail address: szanos@northwell.edu (S. Zanos).
[1] These two investigators contributed equally to this work.

https://doi.org/10.1016/j.brs.2020.09.002

respect to fiber engagement on a single subject basis is essential, both at the time of electrode implantation and during follow up visits with health care providers. Fiber-selective VNS has been demonstrated in experimental animals, but certain stimulation parameters are different for different subjects [19]. Therefore, knowledge of fiber engagement by a set of stimulation parameters is crucial in the process of VNS parameter optimization. The main experimental tool for quantifying fiber engagement in peripheral nerve is registering of stimulus-evoked compound action potentials (eCAPs) through a recording electrode placed at a known distance from the stimulating electrode [20]. The conduction velocities of the different fiber types give rise to characteristic patterns of evoked nerve activity when the nerve is stimulated. These responses are comprised of earlier components, corresponding to activation of different types of faster A-fibers, intermediate components representing B-fibers, and later components for slower C-fibers [21]. Indeed, eCAPs have been used experimentally to optimize stimulation parameters and electrode design in VNS [15,22]. Despite their value, obtaining eCAPs in experimental animals comes with challenges and is generally limited to acute experiments [23]. In clinical applications, registering eCAPs from the vagus nerve is not currently feasible. In principle, a quantifiable physiological response mediated by specific fibers, readily obtainable in experimental animals and in humans, could be used to estimate the magnitude of engagement of those fibers by VNS. For example, B-fiber activity in vagal eCAPs is known to be related to VNS-related changes in heart rate [24]. However, for a set of physiological responses to be useful as markers for vagal fiber activation, data-driven models relating those two modalities need to be compiled and validated. Such models do not exist for VNS.

In our study, we investigated in a rat model the quantitative relationship between activation of different vagal fiber types and several physiological responses to cervical VNS. We chose physiological responses that can be easily and non-invasively obtained in experimental animals and in humans, and that are involved in mechanisms relating to specific vagal fiber types. We characterized the bivariate associations of stimulus-evoked EMG, heart rate changes and breathing changes with A-, B- and C-fiber eCAP components respectively, on a single subject basis and across many subjects. Based on these associations, we built and tested predictive multivariate models that use physiological responses to VNS to estimate the magnitude of activation of different fiber types. These models provide the first quantitative tool for rapid, non-invasive estimation of stimulus-evoked vagal fiber activation that, after further evaluation in animal and human studies, could be used to optimize VNS therapies targeting different organs and diseases on a single subject basis.

Methods

Animal preparation, anesthesia, physiological instrumentation

Thirty adult male Sprague Dawley rats (age 2–5 months and weight between 300 and 550 gm) were used in the study under the approval of the Institutional Animal Care and Use Committee at The Feinstein Institutes for Medical Research. Rats were anaesthetized using isoflurane (induction at 4% and maintenance at 1–2%) and medical oxygen; anesthesia was maintained throughout the experiment. Body temperature was measured with a rectal probe and maintained between 36.5 and 37.5 °C using a heating pad (78914731, Patterson Scientific) connected to a warm water recirculator (TP-700 T, Stryker). ECG was recorded by using 3-lead needle electrodes subcutaneously on the limbs and amplified using a commercial octal bio-amplifier (FE238, ADI). Breathing was monitored by using a temperature probe placed outside of the nostrils along with a bridge amplifier (FE221, ADI); the probe reported changes in air temperature during breathing movements: drop in temperature during inhalation, and rise during exhalation (Fig. 1A and B). All physiological signals were first digitized and then acquired at 1 kHz (PowerLab 16/35, ADI) and visualized on LabChart v8 (all from ADInstruments Inc).

Surgical preparation and vagus electrode placement

To expose the cervical vagus nerve (cVN), a midline 3 cm skin incision was given on the neck (Fig. 1A). Salivary glands were separated, and muscles were retracted to reach the carotid bundle. Under a dissecting microscope, the left or right cVN was isolated first at the caudal end of nerve and then at rostral end of nerve. The middle portion, between the two isolated sites was left intact within carotid bundle to minimize the extent of surgical manipulation and trauma to the nerve. After isolation of the nerve, a custom-made, bipolar or tripolar "Flex" electrode was placed on the caudal site; a second bipolar "Flex" electrode was placed on the rostral site of cVN. Flex electrodes were made use a polyimide substrate and sputter-deposited iridium oxide contacts for low electrode impedances and stable stimulation characteristics [25–27]. Electrode contacts had dimensions of 1418 × 167 μm^2 with an edge-to-edge spacing of 728 μm and center-to-center spacing of 895 μm. Typical individual electrode impedances in saline ranged from 0.5 to 1.5 kΩ. The distance between the stimulating electrode (tripolar: center contact; bipolar distal side contact) to the most proximal recording electrode on the nerve was measured roughly 5–6 mm. Silicone elastomer (Kwiksil by World Precision Instruments) was placed around the cuff to minimize current leakage during stimulation.

Vagus nerve recording and stimulation

Neural activity from each contact on the recording electrode was amplified, digitized (30 kS/s, 16bit resolution) and filtered (60-Hz notch), using a 32-channel RHS2000 stim/record headstage and 128ch Stimulation/Recording controller (Intan Technologies); recordings were single-ended, relative to a ground lead placed in the salivary gland. Nerve stimulation was delivered in constant current mode as trains of monophasic rectangular pulses using an STG4008 stimulus generator (Multichannel Systems). In all experiments characterizing neural and physiological relationship, we initially determined the "neural threshold" (NT) as the lowest stimulus intensity for a 100-μs duration pulses that evoked a discernable evoked potential, which was always within A-fiber latency window (<1 ms), at the proximal recording contact. Most of time (>90%), the evoked response EMG was also observed. The physiological threshold (PT), which evoked visible heart rate/respiratory change, was usually 3 or 4 × NT. Stimulus trains of 10-s durations were then delivered, each with stimulation parameters randomly selected from a range. In particular, pulsing frequency was 30 Hz, pulse width was between 40 and 600 μs, stimulation intensity was between 0.5 and 10 × NT. The stimulation configuration was either tripolar (cathode-center or cathode-corner) or bipolar (cathode-cephalad or cathode-caudad). There were at minimum 15-s long pauses between successive trains to ensure that physiological measurements had fully recovered before a new train was delivered. The different stimulus trains were delivered once per animal, in random order, to limit the total duration of each experiment to 3–4 h and prevent changes of the animal's physiological state due to prolonged anesthesia.

Another set of experiments was conducted to document the physiological responses to different pulsing frequencies and pulse counts. In these experiments, VNS consisted of 10-s long trains of

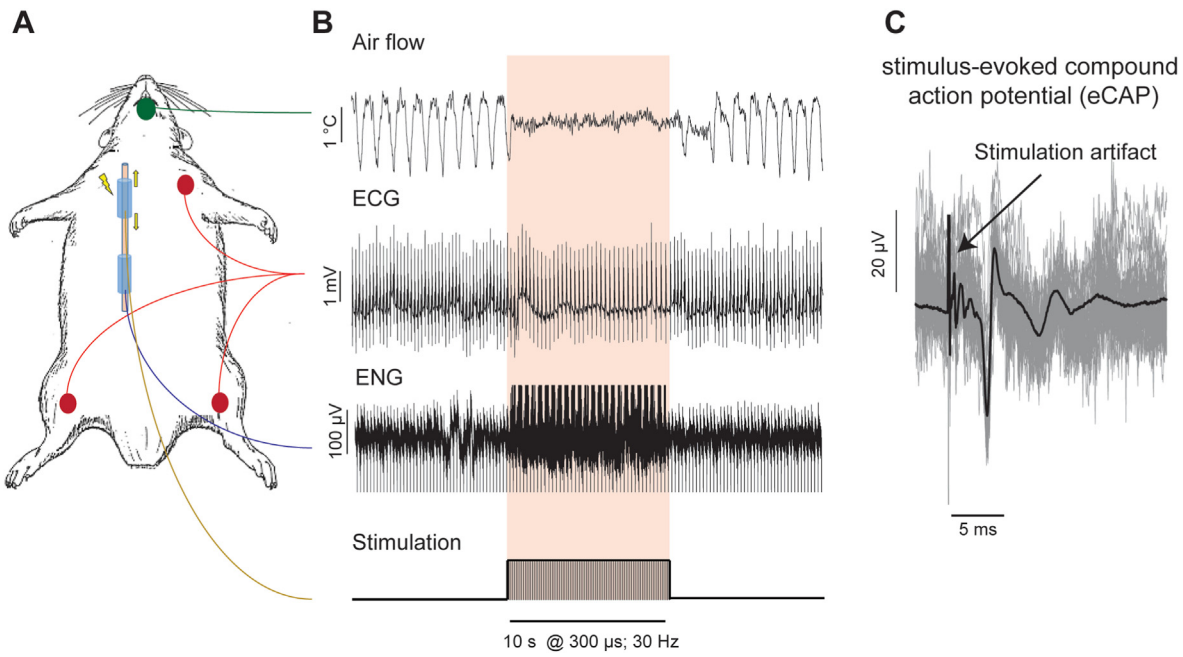

Fig. 1. Electrodes, sensors and physiological signals involved in the experiments. (A) Schematic of an anesthetized animal with the typical locations of vagus nerve cuff electrodes (stimulation: rostral, recording: caudal) and physiological sensors (green: nasal sensor; red: ECG sensors). (B) Representative effects of cervical VNS (top to bottom): cessation of breathing (apnea) in the nasal sensor, drop in heart rate in the ECG and evoked nerve potentials in the electroneurogram (ENG), in response to a 10 s-long VNS train (30 Hz, 300 µs pulses). (C) Individual sweeps of evoked nerve potentials aligned with the onset of stimulus pulse (grey traces), and stimulus-triggered average compound nerve action potentials (black trace), extracted from the ENG in panel B. (For interpretation of the references to color in this figure legend, the reader is referred to the Web version of this article.)

100-µs or 600-µs long pulses, with pulsing frequency between 5 and 300 Hz, and stimulation intensity between 0.5 and 3 × PT. In a subset of these experiments, the same frequencies were tested with shorter trains (2–10 pulses, 0.0067- to 5-s train duration, depending on frequency) and intensities between 1 and 10 × PT.

Identification and analysis of neural and EMG signals

Raw nerve signal traces from both recording contacts were filtered using a 1 Hz high-pass filter to remove the DC component. Stimulus-evoked compound nerve action potentials (eCAPs) elicited from all pulses in each stimulus train were extracted by average individual sweeps of nerve recording traces around the onset of pulses (Fig. 1C). A custom-made buffer amplifier was used to record the induced voltage on the electrode during stimulation. Stimulation artifact was suppressed offline by a recently proposed method which subtracts the trace of the stimulation electrode voltage from the eCAP with proper template matching and an edge effect removal algorithm [28] (Fig. S1, Supplementary Materials).

Given the rough estimation of distance between the recording and stimulation electrodes (5–6 mm), we fine tune the distance in analysis so that the latency windows can align well with the A-, B- and C-fiber prominent peaks with pre-defined conduction velocity ranges for each fiber type (A: 5–120 m/s; B: 2–8 m/s; C: 0.1–0.8 m/s) [21]. Fig. 2A shows representative eCAPs at 3 different intensities: 1 × , 4 × and 10 × NT, including activity of different fiber types and EMG. Signals from both contacts in the recording electrode, proximal and distal to the stimulating electrode, were collected (solid and dashed black traces in Fig. 2A). This allowed us to distinguish between neural and EMG signal components. For the given electrode spacing A- and B-fibers had short latencies (<3 ms), while slower C-fibers occurred at longer latencies (>6 ms) [28]. To discriminate C-fiber components from stimulus-evoked EMG, we reasoned that C-fiber volleys should show a latency difference between the proximal and distal recording contacts, spaced apart by a distance of 895 µm, of 1–2 ms, whereas EMG or line noise-related signals should occur simultaneously on both recording contacts [27] (Fig. 2A, panel III).

We conducted additional experiments to ensure that what we considered nerve fiber activity was not EMG. Vecuronium, a neuromuscular junction blocking agent, was infused intravenously with a bolus dose (0.15 mg/kg) and continuous IV (0.15 mg/kg/min) while the animal was ventilated with 41 breaths per minute and 4 ml tidal volume (SAR-1000, CWE Inc., Ardmore, PA). During vecuronium infusion, the EMG component in the eCAP was considerably suppressed while the neural components were still visible (Figs. S2 and S9, Supplementary Materials). The resulting time window for the majority of the EMG component was 2–6 ms, consistent with other studies documenting VNS-induced laryngeal motor-evoked potential in rats [27–29] (Fig. 2B). We computed A- and B-type fibers amplitudes as the peak prominence and C-type fiber amplitude was defined as the peak-to-trough amplitude of late (>6 ms) eCAP components. The C-fiber component of the eCAP was clearly distinguishable from the EMG-related component at a range of stimulus intensities, as shown by measurements made with and without neuromuscular blocker (Figs. S9A and B, Supplementary Materials). The amplitude of the C-fiber component increased with stimulus intensity, and saturated at intensities of about 8–10 times threshold (Fig. S9C, Supplementary Materials).

Analysis of physiological signals

We computed the magnitude of EMG response from respective eCAPs as the peak-to-trough amplitude of the (typically biphasic) response within the EMG window; that amplitude was then normalized by the mean EMG amplitude in that subject, recorded at a specific set of VNS parameters (based on results shown in Fig. S3, Supplementary Materials): intensity 6–8 × NT, pulse width

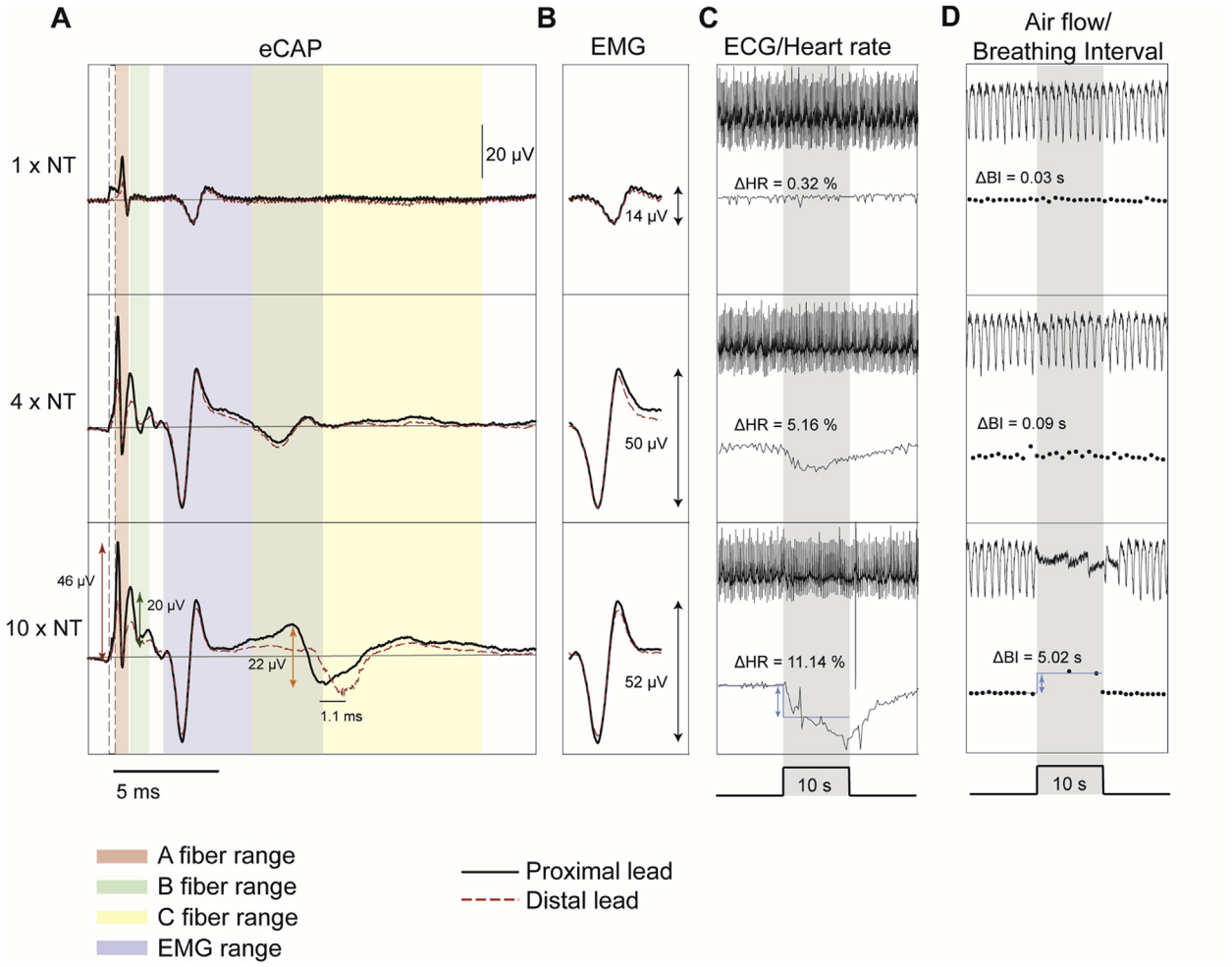

Fig. 2. Quantification of nerve fiber activation by and physiological responses to VNS. Three VNS trains (300 pulses, 300 μs pulse width, at 30 Hz) were delivered at 3 stimulus intensities (1, 4 and 10 times the neural threshold, NT, from top to bottom), and stimulus-evoked compound action potentials (eCAPs), heart rate and breathing responses were registered. (A) Average eCAP responses to single VNS pulses, after stimulus artifact suppression, for each of the 3 VNS intensities. Two eCAP traces are shown, one from each of the recording contacts (black trace for proximal lead to the stimulating electrode, red line for the distal lead). Fiber-specific responses were measured as peak-to-trough amplitude of eCAP components occurring within specific latency windows: A-fiber (0.3 ms–1 ms, red shaded area), B-fiber (0.9 ms–2.2 ms, green area) and C-fiber (5.5 ms–16.7 ms, yellow area); also shown is the window corresponding to stimulus-evoked EMG activity (2.5 ms–10 ms, blue area), partially overlapping with the C-fiber window. Shown at the 10 × NT (bottom) panel are the amplitudes of A-, B- and C-fiber activation (shown in red, green and orange vertical arrows, respectively, along with their values). The relative latency shift in the C-fiber response recorded by the 2 electrode leads (horizontal bar in bottom panel, 1.1 ms), indicates a slow-conducting neural source for this component. (B) Magnitude of stimulus-evoked EMG for the 3 VNS intensities (vertical black arrow) measured as peak-to-trough amplitude of the EMG component of the corresponding eCAPs shown in panel (A). The 2 eCAP traces (black and red) show no relative latency shift, indicating a non-neural source. (C) ECG and heart rate (HR, calculated with each cardiac cycle) traces before, during (grey area) and after delivery of the 3 VNS trains. The HR response (ΔHR) is calculated as the difference between the mean HR before and during VNS, normalized by HR before VNS, and its value is shown in each case. (D) Air flow and breathing interval (BI, calculated with each breathing event) before, during and after VNS. The BI response (ΔBI) is calculated as the difference between the mean BI before and during VNS, and its value is shown in each case. (For interpretation of the references to color in this figure legend, the reader is referred to the Web version of this article.)

600 μs. Using a custom algorithm, ECG peaks corresponding to the R waves were identified, and heart rate (HR) was computed from R-R intervals. We defined stimulus-induced change in HR (ΔHR) as the difference between the mean HR during a 10-s epoch before the onset of the stimulus train ("pre-stimulus") and the mean HR during the stimulus train ("during-stimulus"), divided the mean pre-stimulus HR. In recordings from the nasal temperature sensor, we identified peaks (end of expiration) and troughs (end of inspiration). We defined the interval between two successive peaks (or two successive troughs) as breathing interval (BI). We defined the stimulus-elicited change in breathing interval (ΔBI) as the difference between the mean pre-stimulus and the mean during-stimulus BI. In those experiments in which VNS trains were of short duration, during which less than 2 R-R intervals occurred, we used 5 R-R intervals immediately following the train to estimate mean HR "during stimulus". The measured signals and corresponding derived variables (ECG and ΔHR, and nasal sensor temperature and ΔBI) are shown in Fig. 2C and D.

Regression and prediction models

A bivariate model was used to capture the relationship between A-, B- and C-fiber amplitude and the related physiological variable (EMG, ΔHR and ΔBI, respectively). Individual models were fitted from data for each subject (Fig. 4 A, B and C). After normalizing fiber amplitudes and physiological responses to their maximum values for a given subject, normalized data were used to generate a single bivariate model for each fiber type across all subjects (Fig. 4 D, E and F).

A multivariate quadratic model was compiled for quantitative estimation of relative amplitude of fiber activation (percent of maximum for that subject), using four inputs from all the subjects: EMG, ΔHR, ΔBI, and charge per pulse (Q), defined as the product between pulse width and the current intensity in units of NT. The general form of the model was:

$$\text{Fiber ampl.\%} = a_0\,Q + a_1\,EMG + a_2\,\Delta HR + a_3\,\Delta BI + a_4\,Q^2 + a_5\,EMG^2 + a_6 HR^2 + a_7 BI^2 \quad (1)$$

The model was trained and tested with leave-one subject-out cross-validation. Briefly, the entire dataset was divided in two subsets: training set (data from all subjects except one), to build the model, and the test set (the subject that was left out) to assess model performance. The training procedure was repeated 100 times (100-fold random cross-validation method). To build the model, we selected only those fitted coefficients showing statistical significance (F-test, $p < 0.01$) in at least 50 of 100 times. The last model was developed by taking the medians of the selected coefficients for each input term in Eq. (1). Finally, we computed performance by applying the model on data from the test set.

A 2-term asymptotic exponential model, akin to double exponential function, was computed to capture the relationship between each of the physiological responses (HR or BI) at a pulsing frequency *f* with respect to the same response at 30 Hz ("frequency gain"). The general form of the model was:

$$\text{Frequency gain} = b_0 + b_1 \exp\left(-f/\tau_1\right) + b_2 \exp\left(-f/\tau_1\right) \quad (2)$$

where b_0 is a fitting offset, b_1 and b_2 are the initial values, and τ_1 and τ_2 are the time constants of the exponential functions. The coefficients were optimized using Nelder-Mead simplex direct search method with distinct initial value settings for two exponential terms.

Performance metrics and statistical analysis

To assess goodness-of-fit performance of the different models, the root mean square error (RMSE) and the normalized RMSE values were computed.

$$RMSE = \sqrt{\frac{\sum_i^N (y_i - \hat{y}_i)^2}{N}}, \qquad NRMSE = \frac{RMSE}{\max(y) - \min(y)}$$

where y_i is the observed value for the i-th observation, $\hat{y}_i$ is the predicted value and N is the length of the observation.

After building the linear quadratic model for each fiber type, we computed RMSE values. Chance performance level was set with a permutation test [30]. We created surrogate data sets from the test data by randomly shuffling the fiber-type label of each data point, thereby destroying any relationship between inputs and outputs. Then, we treated the surrogate dataset just like the original data and computed the RMSE using the final models. By repeating this process 100 times, we created a distribution of "random performance" metrics; we considered model performance computed on the original data significant if it was smaller than the 5th percentile of the random performance RMSE distribution.

The non-parametric Kruskal-Wallis test (KWT) was used to compare different fiber activation evoked during VNS. A p value less than 0.05 was considered statistically significant. All the analyses were performed using MATLAB 2017b software (MathWorks, Natick, MA, USA).

Results

Neural and physiological responses to VNS

We wished to infer the magnitudes of A-, B- and C-fiber activation by using physiological responses to VNS that can be measured rapidly and noninvasively in human subjects and experimental animals. We delivered cervical VNS with different stimulation parameters known to engage different fiber types. Through a second recording electrode, also placed on the cervical vagus, we registered stimulus-evoked compound nerve action potentials (eCAPs) and A-, B- and C-fiber responses, as well as laryngeal EMG responses, were extracted. At the same time, we monitored ECG and nasal air flow and calculated the magnitude of VNS-elicited changes, from a pre-stimulation baseline level, in heart rate (ΔHR) and in breathing interval (ΔBI). Intensity threshold values for neural (typically A-fiber) activity ranged between 12 and 30 μA (mean ± SD: 22.5 ± 6 μA) for 100 μs-long monophasic pulses.

To characterize the relationship between vagal fiber activation and physiological responses, we first documented how they both changed in response to VNS of different stimulus intensities, pulse widths and pulsing frequencies. Across all subjects, the mean (±SD) amplitude of A-, B- and C-fiber responses were 59.01 ± 42.60 μV, 21.11 ± 15.33 μV, and 74.80 ± 73.70 μV, respectively. The mean (±SD) latencies of fiber activity peaks were 0.4192 ± 0.0126 ms for A-fibers, 1.2315 ± 0.1777 ms for B-fibers, and 9.7688 ± 1.4885 ms for C-fibers (Fig. S7, Supplementary Materials). The mean (±SD) magnitude of evoked EMG, ΔHR and ΔBI responses were 57.03 ± 74.03 μV, −9.64 ± 12.27%, 2.64 ± 4.59 s, respectively: the typical physiological responses to VNS were therefore muscle contraction, slowing of the HR and prolongation of the BI. The physiological responses elicited by VNS were statistically different from the corresponding physiological measurements during the 10 s-long pre-stimulation baseline, for all threshold and supra-threshold intensities (upper-tail one-sided statistical *t*-test, $p < 0.001$ for all 3 comparisons: EMG_{VNS} vs. EMG_{base}, HR_{VNS} vs. HR_{base} and BI_{VNS} vs. BI_{base}).

A-fiber amplitude and EMG magnitude both increased with increasing stimulus intensity (Fig. 3A, left and middle panels), with a linear relationship between them that was preserved across stimulus intensities (Fig. 3A, right panel). Similarly, B-fiber amplitude and ΔHR magnitude also increased with increasing stimulus intensity (Fig. 3B, left and middle panels), but this time the fiber amplitude-response magnitude relationship had an exponential form (Fig. 3B, right panel). C-fiber amplitude and ΔBI magnitude started building up at significantly higher stimulus intensities (Fig. 3C, left and middle panels) and an exponential relationship between C-fiber activation and the slowing of breathing was typically seen (Fig. 3C, right panel).

Relationships between fiber amplitudes and physiological response magnitudes

We then quantified the relationship between A-, B-, and C-fiber amplitude and the magnitude of EMG, heart rate (ΔHR) and breathing interval (ΔBI) responses, respectively. Based on our previous observations, we used a linear model to relate A-fiber amplitude to EMG magnitude. In all subjects, A-fiber amplitude and magnitude of EMG response were positively and linearly correlated (Fig. 4A). By normalizing the neural and the EMG responses by their maximum values within each subject, we were able to fit data from all subjects with a single linear function (Fig. 4D). Normalized values of A-fiber amplitude and EMG magnitude generally increased with increasing charge per pulse (stimulus intensity × pulse width) of the pulses within a given stimulus train (Fig. 4D). Using a similar

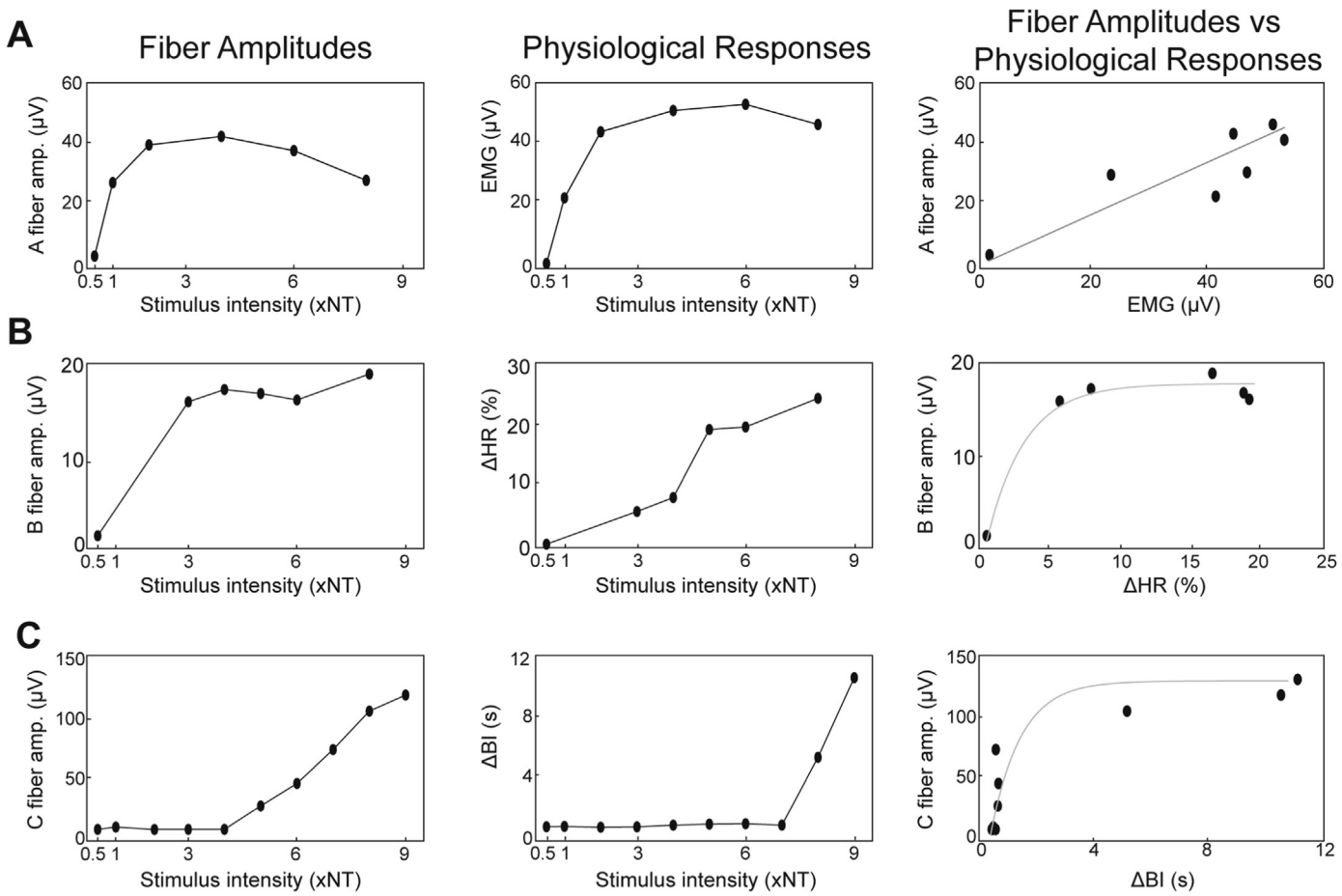

Fig. 3. Nerve fiber activation and physiological responses with increasing stimulus intensity. Data are from the same subject in which VNS was delivered in trains of 300 pulses, 100 μs pulse width, at 30 Hz. (A) Amplitude of A-fibers (left panel) and magnitude of stimulus-evoked EMG (middle panel) plotted as a function of stimulus intensity ("capture curves"), in units of neural threshold (NT). Plotting the same data as A-fiber vs. EMG pairs reveals a linear relationship (right panel). (B) Capture curves of B-fibers (left) and heart rate responses (ΔHR, middle), and exponential relationship between them (right). (C) Capture curves of C-fibers (left) and breathing interval responses (ΔBI, middle), and exponential relationship between them (right). Note that C-fiber and ΔBI responses are captured at higher intensities.

procedure, we related B-fiber amplitude to ΔHR magnitude. In this case, an exponential model was used to fit the data for individual subjects (Fig. 4B) and, after normalization, collectively for all subjects (Fig. 4E). Again, normalized B-fiber amplitude and ΔHR generally became greater as charge increased (Fig. 4E). We repeated these steps for C-fiber amplitude and ΔBI magnitude and used an exponential model to fit the data (Fig. 4C and F). In this analysis, data from several stimulus trains were omitted since in C-fibers were not always activated and/or there was not always a breathing response to VNS. This resulted in a smaller dataset than those of A- and B- fibers. These bivariate correlations were similar in shape between bipolar and tripolar stimulation electrode configurations (Fig. S10, Supplementary Materials).

To assess goodness of fit, we computed the normalized root mean square error (NRMSE) values for each single-subject fit, for each of the 3 fiber amplitude-physiological response magnitude models. Median NRMSE was 0.173 (range: 0.085–0.266) for the A-fiber vs. EMG model, 0.192 (0.119–0.232) for the B-fiber vs. ΔHR model, and 0.098 (0.044–0.179) for the C-fiber vs. ΔBI model (Fig. 4G).

A- and C-fiber activation associated with breathing responses

Despite our finding of an association between C-fiber amplitude and magnitude of the breathing response (ΔBI), it is known that breathing is affected in distinct ways by afferent A- and by C-fibers [31]. We further characterized the relationship between A- and C-fiber amplitude, and ΔBI. We classified breathing responses to individual VNS trains in 3 groups: "bradypnea", if ΔBI was >0.2 s and 2 or more breathing events occurred during the 10-s long stimulus train, "apnea", if 1 or no breathing events occurred during the stimulus train, and "no change in breathing", if ΔBI was <0.2 s (Fig. 5A). For each VNS train, the amplitudes of A- and C-fiber activity were normalized to their maximum values in the corresponding subject. We found that A-fibers were roughly equally activated in apnea and bradypnea ($p = 0.83$, KWT), while there was significantly greater A-fiber activation in bradypnea responses vs. no change in breathing ($p < 0.01$, KWT). On the other hand, there was significantly greater C-fiber activation in apnea compared to either bradypnea or no change in breathing ($p < 0.001$, KWT for both comparisons) (Fig. 5B). These findings suggest that moderate changes in the breathing pattern are typically associated with activation of A-fibers alone. However, apnea responses were frequently associated with C-fiber activation. Since non-fiber-selective stimulation waveforms were used in this study, C-fiber activation could happen alone or, most likely, in combination with A-fiber activation.

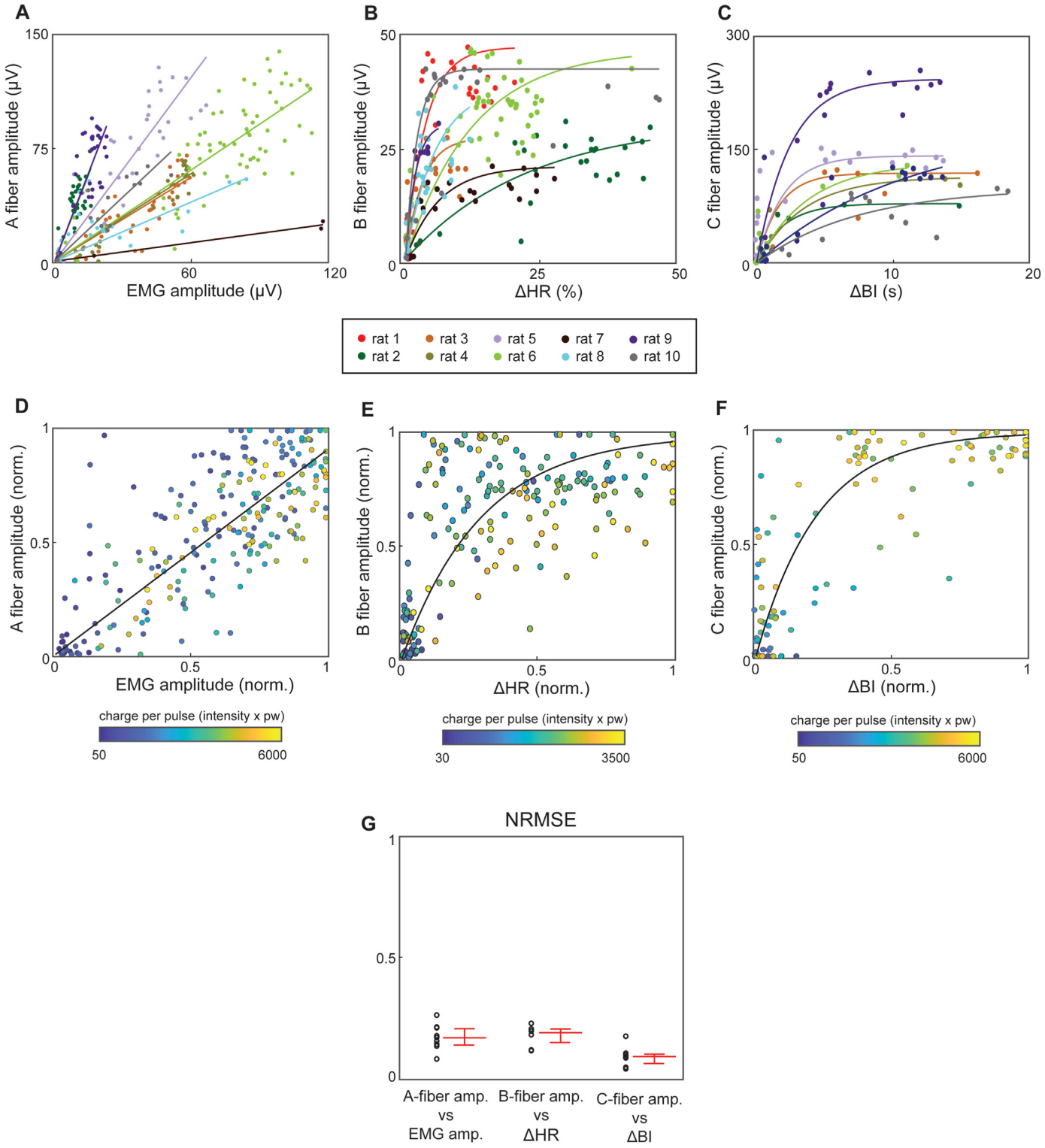

Fig. 4. Relationships between nerve fiber activation and physiological responses. (A) Relationship between A-fiber amplitude and magnitude of stimulus-evoked EMG, in each of 10 subjects. Each dot represents an A-fiber vs. EMG measurement pair from a single VNS train. Colors represents different animals, and each curve represents the best linear fit for the data from that animal. (B) Relationship between B-fiber amplitude and magnitude of the heart rate response (ΔHR). Individual curves represent single exponential fits. (C) Relationship between C-fiber amplitude and magnitude of the breathing interval response (ΔBI). (D) Same data as in panel (A), but after each data pair was normalized to the maximum values registered in the corresponding animal. Color represents relative charge per phase (stimulus intensity in units of neural threshold (NT) × pulse width in μs), ranging from 0.5 × NT at 100 μs(blue) to 10 × NT at 600 μs(yellow). Curve represents a linear fit model. (E) Similar as (D), but for normalized values of B-fiber activation and ΔHR response. Curve represents a single exponential fit model. (F) Similar as (D), but for normalized values of C-fiber activation and ΔBI response. Curve represents a single exponential fit model. (G) Normalized root mean square errors (NRMSE) for each of the individual fits shown in panels (A) (A-fiber amp. vs. EMG), (B) (B-fiber amp. vs. ΔHR) and (C) (C-fiber amp. vs. ΔBI). Single dots represent the NRMSE associated to each subject for the three models. Barplots report the median and the interquartile range of all NRMSE values within each model. (For interpretation of the references to color in this figure legend, the reader is referred to the Web version of this article.)

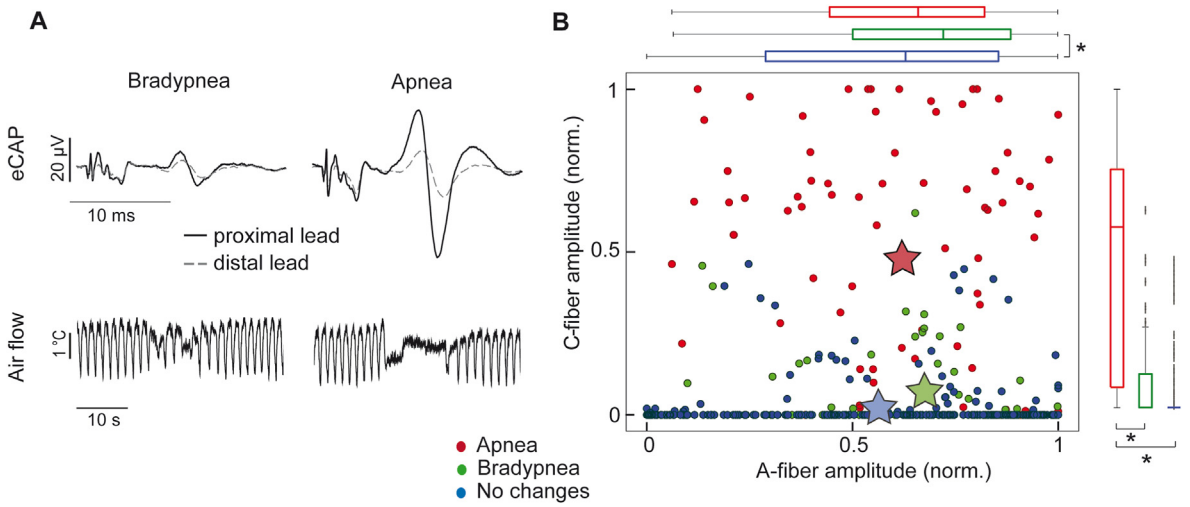

Fig. 5. A- and C-fiber activation associated with breathing responses. (A) Example average eCAP traces from the two recording electrode contacts (solid black from proximal, dashed grey from distal lead) and corresponding breathing response, in a case of bradypnea (left panels) and apnea (right panels). (B) Scatter plot of pairs of A-fiber vs. C-fiber amplitudes recorded in 10 subjects, color-coded by breathing response group: apnea (red dots), bradypnea (green dots) and no effect in breathing (blue dots). Fiber amplitudes are normalized to the maximum value registered in each subject. Stars represent the center the 2-D distributions for each of the 3 breathing response groups, and boxplots represent the median and interquartile range of A- and C-type fiber amplitudes for each of the 3 groups (*: $p < 0.01$ Kruskal Wallis test). (For interpretation of the references to color in this figure legend, the reader is referred to the Web version of this article.)

Models to estimate vagal fiber activation

We then attempted to estimate quantitatively the percentage of the A-, B- and C-fiber activity evoked by VNS, by considering the magnitude of the observed physiological responses and some stimulation parameters. For that purpose, we built multivariate quadratic models (Eq. (1)) using four independent variables: Normalized EMG amplitude, ΔHR, ΔBI, and stimulus charge per pulse (normalized intensity × pulse width). Among all physiological readouts, EMG require normalization within subject because the magnitude range varies significantly across different animals, and the reference was consistently selected from the stimulation parameter, 6–8 × NT, 600 μs, which generally has maximum EMG response (Fig. S3, Supplementary Materials). Table 1 shows the significant coefficients for each model. After models were computed, chance performance levels were determined by means of surrogate distributions and were used to determine significance of model performance.

Regarding model performance, RMSE for A-, B- and C-fiber models were significantly better than chance, for both training and test data sets (Fig. 6A, B, C). Individual estimated and measured fiber activation percentage from all animals as test data sets are shown in Fig. 6D, E, F; data points in A- and C-fiber models (Fig. 6D and F) are generally closer to unity line, and therefore more accurate, compared to the B-fiber model (Fig. 6E). Additionally, Table S1 reports the amount of variance explained (R^2 value) for the 3 fiber models in each subject. Finally, to understand the effect of each single predictor, we reported in Table S2 the Proportional Reduction of Error (PRE) as suggested in Ref. [32]. Briefly, we computed the error as the residual sum of squares (RSS) obtained with the model A (augmented, using all the predictors) and the model C (compacted, without one predictor) to see the effect of each parameter using the following formula: $PRE = 1 - RSS_A/RSS_C$.

Scaling of physiological responses with pulsing frequency

Our fiber amplitude estimation models depend on physiological responses elicited by VNS at 30 Hz, a pulsing frequency commonly used in clinical VNS. In order to generalize these models to other frequencies, we performed experiments to quantify how physiological responses change with frequency, from 5 to 300 Hz. The ΔHR response increases with increasing frequency, reaches maximum at 50–100 Hz and then it declines (Fig. 7A). In contrast, the ΔBI response shows an abrupt increase that saturates around 50–100 Hz (Fig. 7B). Stimulus-evoked EMG activity did not change with pulsing frequency, as its time-course is shorter than typical inter-stimulus-intervals (Fig. S5, Supplementary Materials), and was not subjected to this analysis. We used 2-term exponential functions (Eq. (2)) to create a "frequency gain" model that translates the physiological response (ΔHR or ΔBI) observed at a given frequency to that observed at 30 Hz (Fig. 7C, and Table 2 with better precision). This translation allows the estimation of vagal fiber amplitudes, using the previously established fiber activation models, for any pulsing frequency. Individual data points used in compiling these models are shown in Fig. S4 (Supplementary Materials). Even though the physiological responses scale with stimulus intensity, their dependence on pulsing frequency is stable. When short-duration stimulus trains were delivered, ΔHR response had a similar dependence on frequency (Fig. S6A, Supplementary Materials), and generally increased with pulse count (Fig. S6B, Supplementary Materials). However, no significant ΔBI responses were documented for trains shorter than 5–10 s (data not shown).

Discussion

In recent years, quantification of the engagement of different fiber types by VNS has been pursued systematically by recording stimulus-evoked compound nerve action potentials (eCAPs) directly from the nerve [15]. Even though several chronic VNS

Table 1
Significant coefficients of the linear and quadratic terms in each of the models for estimating fiber activation, according to the general form of Eq. (1).

Model	Q	EMG	ΔHR	ΔBI	Q^2	EMG^2	$ΔHR^2$	$ΔBI^2$
A-fiber %	–	88.31	–	4.15	–	−21.98	–	–
B-fiber %	–	86.94	2.87	6.52	–	−34.66	−0.042	–
C-fiber %	0.017	−24.29	–	6.11	–	–	–	–

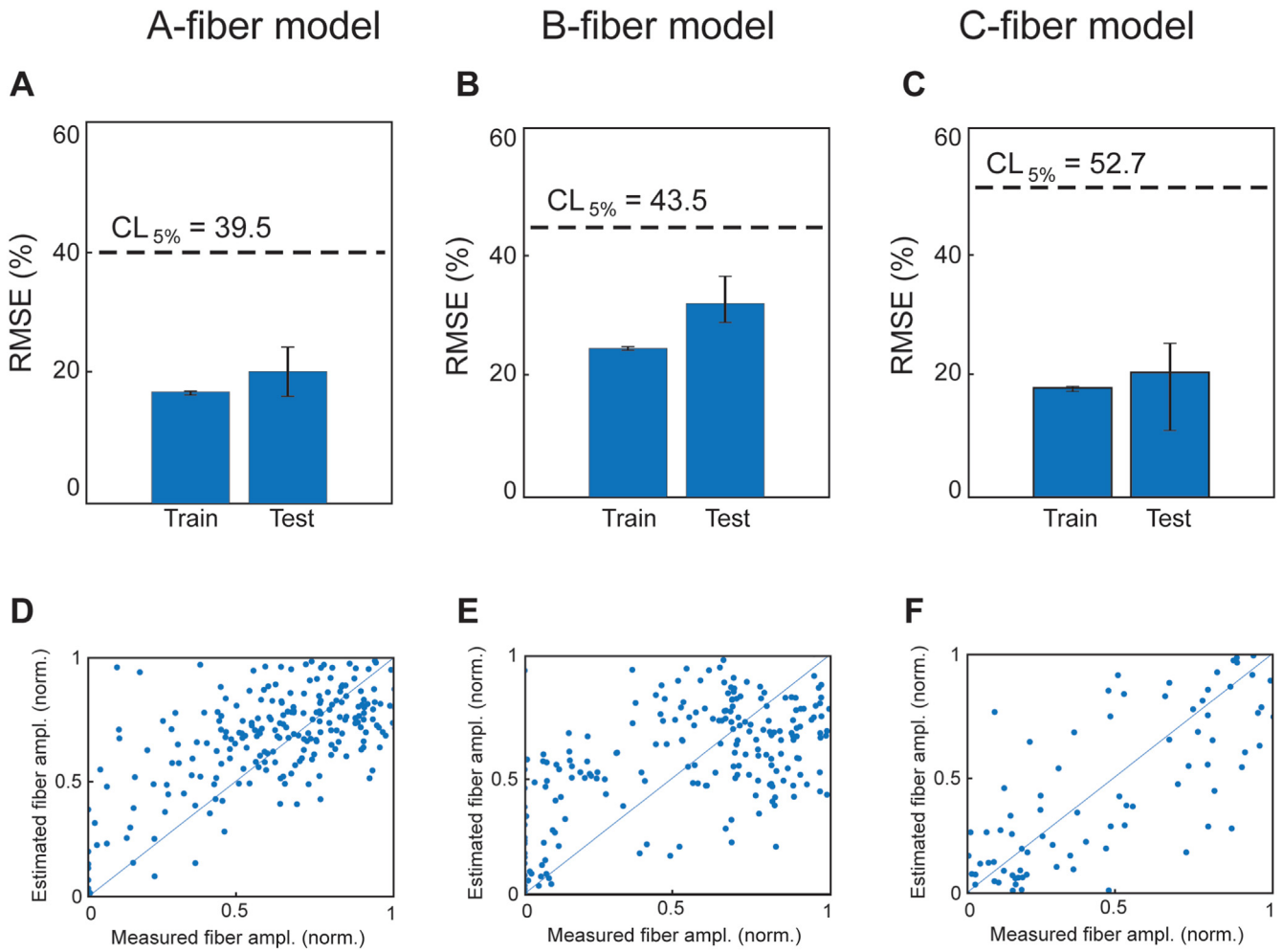

Fig. 6. Performance of models to estimate A-, B and C-fiber activation. (A) RMSE of the A-fiber model for both train and test sets. Bars represent median RMSE and error bars the interquartile range. The horizontal dashed line indicates chance level, as computed by a permutation test. (D) All actual (measured) A-fiber activation percentage and corresponding estimated using the final A-fiber model from Table 1. (B and E) Same as (A and D) but for B-fiber model. (C and F) Same as before, but for C-fiber model.

paradigms have been tested in various animal models of disease [13,33–35], no stable nerve recordings with longevity and stability have been demonstrated [23], and recording eCAPs from the human vagus is not currently feasible. Placement of extra nerve electrodes for recording might increase the risk for surgical complications, accentuate tissue response or affect the integrity of nerve fibers [36]. Given those limitations, a method to quantitatively estimate the level of fiber engagement by cervical VNS using

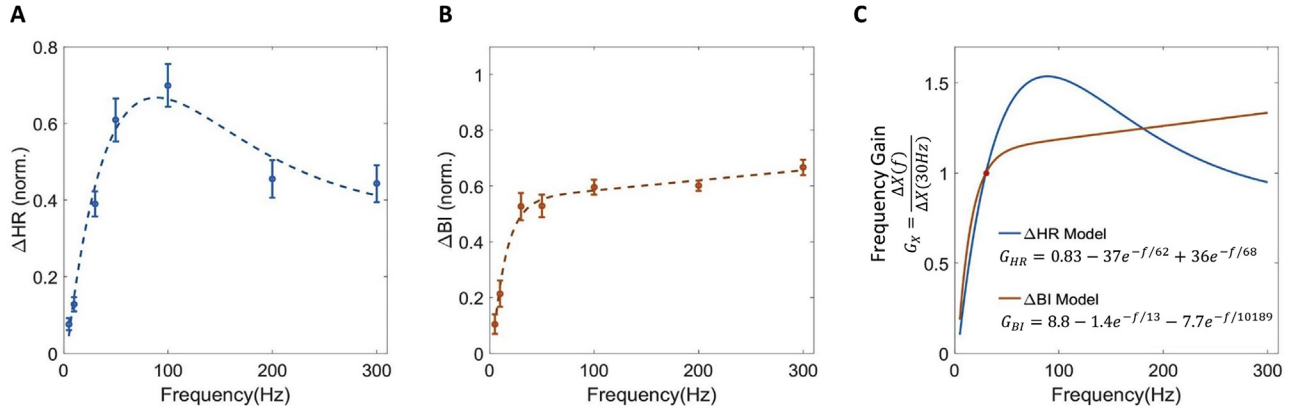

Fig. 7. Scaling of physiological responses with pulsing frequency. (A) Dependence of the heart rate response (ΔHR) on pulsing frequency. Individual points and error bars represent the average and standard error, respectively, of ΔHR responses to VNS trains of a given pulsing frequency with different amplitudes and pulse widths, across 5 animals. Dash line represents the fit line using a 2-term exponential model. (B) Same as in panel (A), but for the breathing interval response (ΔBI). (C) Graphical representation and mathematical equation of the "frequency gain" model for ΔHR and ΔBI, with "unity gain" corresponding to the responses at 30 Hz.

Table 2
Coefficients of the nonlinear 2-term asymptotic exponential function for each of the 2 physiological responses (ΔHR and ΔBI), that allow calculation of the "frequency gain" in Eq. (2).

Model	b_0	b_1	τ_1	b_2	τ_2
ΔHR(*f*)	0.8298	−37.1404	62.9058	36.1449	67.8152
ΔBI(*f*)	8.7648	−1.3683	12.9306	−7.6528	10,189

physiological parameters that, ideally, can be registered non-invasively, would be of use in preclinical and clinical research, and eventually in the clinical practice of VNS. To the best of our knowledge, ours is the first study to establish such a quantitative estimation method, even though attempts have been made to relate B-fiber activity to changes in heart rate [37] and to qualitatively calibrate functional thresholds for vagal fiber engagement [38].

First, we examined the feasibility of predicting the level of activation of different fiber types using physiological variables with a univariate (linear and nonlinear) regression model. The selection of physiological responses to be correlated with activation of each fiber type was based on established physiological functions of the vagus and on our own past studies [28]. We then compiled a data-driven model for each fiber type that estimated the amplitude of its activation by using corresponding physiological responses, and in the case of C-type fibers, the amount of injected charge. Performance of each of the models was evaluated with data not used in the building of that model, quantified and compared to the chance performance level. The three models are simple, intuitive and in line with what we expected: A-fibers are related to only the observed EMG amplitude, B-fibers to both the heart rate (HR) response and EMG amplitude, and C-fibers to both the prolongation of the breathing interval (BI) and to the injected charge per phase.

VNS evoked fiber activity and physiological responses

The linear relationship between VNS-elicited EMG activity and evoked A-fiber amplitude (Fig. 4A, D) agrees with what is known about the vagal innervation of laryngeal muscles and the effects of VNS on their contraction. Efferent A-fibers in the superior and recurrent laryngeal nerves, both being branches of the cervical vagus, innervate intrinsic muscles of the larynx and account for a majority of large myelinated fibers in the trunk of the cervical vagus [39]. Electrophysiological studies have shown that activation of A-fibers by VNS leads to contraction of laryngeal muscles, and; in patients with cervical vagus implants, high stimulation intensities produce laryngospasm [40,41]. By comparing eCAPs with and without a neuromuscular blocker (Fig. S2, Supplementary Materials), we established that VNS-elicited EMG occurs 3–10 ms post-stimulus, consistent with monosynaptic activation of innervated muscles. It is worth noting that A-fiber amplitude in these experiments reflects activation of both efferent and afferent A-fibers, which convey sensory information from the lungs. In our experiments, the recording electrode was placed caudally to the stimulating electrode and the stimuli were delivered in the cathode-caudad polarity, promoting the activation of efferent fibers [43]. Using this configuration, it is likely that a significant part of the A-fiber component corresponds to activation of efferent A-fibers, as some of the afferent A-fiber activity is blocked by the hyperpolarizing anode [43]. This would explain the relatively strong linear relationship between A-fiber amplitude and EMG activity, and the weaker relationship with changes in breathing (Fig. 5). The use of normalized EMG values in the model minimizes variability introduced by the method for recording or analyzing EMG activity. Interestingly, EMG responses were documented at significantly lower intensity levels than HR or breathing responses. This suggests that one can get measurable EMG, and therefore somatic afferent Aβ fiber activation, at lower intensities than those producing heart rate changes (B-fibers) or breathing changes (Aδ and C fibers). This has implications for the use of vagal evoked potentials, evoked cortical activity or fMRI changes for measuring afferent vagal activation and optimizing VNS-based neuroplasticity paradigms [44], as part of those cortical responses could reflect "myogenic" sources. Finally, it is known that laryngeal EMG is evoked first by activation of fibers of the recurrent laryngeal nerve, located inside the cuff, and eventually by activation of the superior laryngeal branch located outside the cuff through current leakage [45,46]. Even though measures were taken to provide additional insulation to the neural interface in our experiment, it is likely that the linearly increasing evoked EMG results from co-activation of hypoglossal nerve and pharyngeal branch fibers by leaking current, especially at high stimulation intensities.

We found that B-fiber activation by VNS is related to HR drop (Fig. 4B, E), in agreement with findings in other animal studies [37,38,47]. Indeed, the vagus innervates the sinoatrial and the atrioventricular nodes, with negative chronotropic and dromotropic effects, respectively [48–50]. Studies in humans suggest that bradycardia is elicited by increasing VNS intensity or pulse width, both consistent with B-fiber activation [51]. The relationship between B-fiber activation and HR drop is not linear, but exponential (Fig. 4B, E). This suggests that fiber types with higher activation thresholds, like C-fibers (Fig. 3B and C) may contribute to the cardio-inhibitory effect of VNS beyond maximum activation of B-fibers. Bradycardia can indeed be induced by selective stimulation of efferent C- fibers [52,53], whereas activation of afferent fibers, probably A- and C-type, can decrease HR by centrally enhancing parasympathetic efferent outflow and reducing sympathetic efferent outflow [47]. Finally, optogenetic activation of vagal A- and C-type afferent fibers caused bradycardia [31]. In our study, quantifying the B-fiber response was challenging because its amplitude was small and its latency was short, in some cases neighboring the A-fiber response. For these reasons, we sometimes had to measure the B-components in eCAPs manually and that could be partially responsible for the somewhat lower estimation accuracy of the B-fiber model (Fig. 6D, E, F).

We analyzed the effects of VNS on breathing and quantified their relationship to A- and C-fiber activation. C-fiber amplitude correlates strongly with breathing changes: weak C-fiber activation was associated with slower breathing during VNS, whereas strong C-fiber activation with apnea (Fig. 5A and B). C-fibers were engaged at relatively large charge injections (Fig. 4F), reflected in the coefficient assigned to charge per phase in the C-fiber model (Table 1). A-fibers were sometimes associated with breathing changes, but that relationship was not as consistent: the amplitude of A-fiber activation during bradypnea was significantly greater compared to lack of breathing response (Fig. 5B). Our findings are consistent with the known role of afferent A- and C-fibers in the neural regulation of breathing [54,55]. Stimulation of A-fibers leads to a decrease in breathing rate through inhibition of the central inspiratory drive [56], a response happening normally as part of the Herring-Breuer reflex [57]. Our recording and stimulation configuration minimized the afferent component of evoked A-fiber activity, hence the lack of consistent relationship between A-fibers and breathing changes. Similarly, stimulation of C-fibers leads to decrease of tidal volume, increase of respiratory rate, constriction of airways, and defense reflex associated with coughing [58]. Fiber engagement in VNS with rectangular waveforms, like those used in our study, follows a size principle [59] (Fig. 3): small stimulation intensities and/or short pulse widths activate A-fibers and lead to moderate prolongation of the BI (Fig. 5B), whereas higher

intensities and/or longer pulse widths are more likely to engage both A- and C-fibers, resulting in a combined inhibitory effect on breathing and either greater prolongation of the BI or apnea (Fig. 5B).

VNS configuration and parameter selection

In our study, we used monophasic pulses, as they result in shorter and simpler artifact shapes and yield better artifact suppression for eCAPs. The monophasic design can also prevent the confounding of the second phase acting as "cathodic" on the return electrode which might initiate action potentials from a different point. Monophasic pulses are associated with modestly lower thresholds for all fiber types [60]. They are also not common in clinical applications, for the purpose of charge-balancing and chronic neural interface safety. For these reasons, and given the clinical necessity for biphasic pulses, it is likely that the relationship between nerve fiber activation and non-invasive physiological measures in humans will be more complex.

In terms of stimulation waveform, we used square pulses, of different intensities and pulse widths, that generally do no selectively engage fiber types; instead, fiber recruitment follows a size principle: fiber with the largest diameter (A-type) and recruited first and those with the smallest diameter (C-type) are recruited last. Several stimulation strategies, such as temporal patterning [24], asymmetrical waveforms [61], have been used to reverse this order. Furthermore, in large animals, multi-contact electrode have been shown to elicit different physiological responses depending on which fascicle was targeted [62]. Some of studies also show good correlations between different fiber components and physiological responses [24], implying that our model may not be relevant only to square pulses and the "default" recruitment order, but may be generalizable to different stimulation parameters. In that sense, it will be interesting to test the validity of our models under conditions of fiber type- or fascicle-selective VNS.

The VNS trains used in the modeling part of our study had a fixed pulsing frequency of 30 Hz. Even though 30 Hz is common in preclinical and clinical studies, it is known that pulsing frequency has a significant effect on physiological responses, both afferent [63] and efferent [64]. At the same time, it does not affect nerve responses to single pulses, due to lack of temporal summation (Fig. S5, Supplementary Materials). That means that the fiber models, as they were (Table 1), would not translate to other frequencies. In order to make the models generalizable to other frequencies, we computed formulas that re-scale the relevant physiological responses to those observed at 30 Hz (Fig. 7 and Table 2). These formulas rely on responses observed during 10 s-long trains (or during the first 10 s of longer VNS trains). Even though train durations <10 s are uncommon in experimental or clinical VNS studies, we found that shorter trains had similar effects on the HR response (Fig. S6, Supplementary Materials) but not on the BI response, which required train durations of at least 5–10 s (data not shown).

Limitations

Our study has several limitations. First, the experiments were performed under isoflurane anesthesia. It is unlikely that anesthesia affects eCAPs, as those depend on the excitability of axons close to the stimulating electrode. However, it almost certainly affects the physiological responses to VNS: isoflurane suppresses motor vagal activity to the heart [65] and lungs [66], it suppresses afferent and efferent arms of the baroreflex [67] and is a potent depressant of respiratory function [68]. Therefore, it is likely that the coefficients of the models compiled in this study will be different in awake subjects, or in subjects anesthetized with different agents. It is also likely that the use of isoflurane in our study is partly responsible for the relative absence of tachycardia responses to VNS, seen in other papers not using isoflurane [69]. For that reason, the B-fiber-bradycardia association may be less obvious in situations where the vagal circuits involved in these responses are less affected by anesthesia, or it may be more dependent on stimulation parameters. For example, smaller intensities may produce tachycardia, due to activation of sympathetic vagal fiber or vagal-sympathetic reflexes [69], whereas higher intensities may still produce bradycardia. Given the noninvasive nature of the physiological measurements used in the models we propose, future experiments in awake, behaving animals using a wide range of stimulation parameters will be needed to address this source of variability.

Our analysis is based on the assumption that fiber engagement and eCAP amplitude are linearly related. However, studies have shown that the distribution of nerve fibers is non-uniform within the cervical vagus nerve, even in the relatively simple rodent nerves [70,71]. Fibers that lie closer to the stimulating or recording electrode are easier to be excited or contribute more heavily to the eCAP measurements; both effects are more prominent with larger fibers. As the electrode in our study only directly interface a part of the nerve trunk, there is a chance that some fibers contribute more than others to the eCAP signature or to the physiological response, in a manner inversely proportional the location to those fibers relative to the recording or stimulating electrode. This might inevitably lead to errors while quantifying the relationship between eCAP-resolved fiber engagement and physiological effects. These relationships were similar between bipolar and tripolar stimulating electrode configurations (Fig. S10, Supplementary Materials), so the electrode geometry itself did not appear to introduce a significant confounding factor to these models. It is noteworthy that, even though the absolute error of the proposed models was 20–30 (for an output 0–100), the relative error depends on the level of fiber recruitment: for a recruitment level of about 20%, the median relative error would be 42% for A-fibers, 50% for B-fiber and 40% for C-fibers.

Several limitations arise from the choice of the rat as our animal model, which posed constrains on the distance between the stimulating and recording sites (typically 5–6 mm). As the distance was measured with a mm accuracy, which introduces uncertainty around the exact latency windows, in each experiment, the latency window corresponding to each fiber type was defined on the basis of the conduction velocity range for that fiber type [72], while taking into account the actual, measured latency of the pre-eminent peak of the respective eCAP component. This accounted essentially to a slight "fine-tuning" of the latency window for a fiber type to encompass a clear eCAP component corresponding to that fiber type, when such a component was present. This short distance also limits our ability to resolve activation of the several A-fiber subtypes, each with different physiological functions and conduction velocities [72]. At this distance, the faster A-fibers, Aα (motor efferent) and Aβ (somatic sensory from laryngeal muscles and ear), would have latencies around 100 μs. With stimulus pulse widths over 100 μs and a sampling period of 33 μs, detecting these components was not feasible. The A-fiber amplitude we measure likely encompasses slower A-subtypes, Aγ (motor efferents) and Aδ (aortic baroreceptor afferents and lung stretch receptors), with expected latencies of 100–1000 μs. The latencies of the A-fiber peaks in our measurements were within that range (Fig. S7, Supplementary Materials). Amplitude measurements of slower A-subtypes and of B-fibers may also confound each other, as those fiber types have overlapping conduction velocities; moreover, activation of those fiber types has similar effects on heart rate [73].

Despite the use of a slightly slower-than-standard latency window for B-fibers and a peak-to-trough (rather than trough-to-peak) method for measuring B-fiber amplitude (Fig. 2), which typically shifted that measurement to a latency beyond the A-fiber range, it is likely that our cardioinhibitory "B-fiber" model reflects to an extent activation of Aδ fibers and the effects of their activation.

Some of the issues with "blurring" amplitude estimates between different fiber types could be addressed in a large animal, rather than a rodent, model in which the distance between the stimulating and recording site can be significantly longer [15]. It is likely that the resolution of eCAP components at a more "expanded" temporal scale in the large animal model will result in different, and more accurate, model coefficients. In addition, the relatively "simple" anatomy of the vagus in rodents, with one or two fascicles, is different than the multi-fascicular anatomy found in large animals and in humans [70]. This fascicular organization of the human cervical vagus will likely affect the coefficients of the models, as different fascicles seem to contain populations of different fiber sub-types [70]. Finally, given the lack of a clinical, fully implantable recording vagus electrode, collecting detailed eCAP and physiological measurements in humans outside of the operating room is currently not feasible; intra-operative experimental sessions are a possibility but those would be limited in time and will likely not generate enough data to train models that generalize well. For all those reasons, documenting eCAPs and physiological effects of VNS in a representative large animal model, like the swine [70], will be essential to understanding the clinical application potential of our approach.

Applications and future works

The proposed modeling approach can potentially be leveraged as a tool to estimate fiber activation in current and future therapeutic applications of VNS. All physiological parameters used in the models can be non-invasively measured in humans: laryngeal EMG with recording electrodes placed on the skin of the neck [41], HR with standard ECG techniques, and BI with a respiratory belt. The physiological responses used in our models have all been described in human VNS studies [74], even though they will certainly be quantitatively different. The A-fiber estimate could be used to minimize off-site effects of VNS like voice alteration, coughing and paresthesia [75]. Estimation of B-fiber engagement by VNS could facilitate the optimization of stimulation paradigms to treat heart failure [18] or cardiac arrhythmias [76]. Estimation of C-fiber engagement could be used as an index of therapeutic effect in anti-inflammatory applications of VNS [17] Furthermore, estimation of vagal fiber activation, done in real time, could be used in a closed-loop system for optimizing or recalibrating a VNS therapy targeting a specific fiber type while minimizing activation of other fiber types [77]. Finally, patterns of estimated fiber activation could be used in prospective clinical studies as predictors of other, more long-term physiological and clinical effects of VNS.

Funding

The research was supported by a grant to SZ from United Therapeutics Corporation (MD, US).

Data and materials availability

The data that support the findings of this study are available from the corresponding author upon reasonable request.

Code availability

The code used for the data analysis and modeling are can be cloned from https://github.com/ychang3/VNS-Fiber-Engagement.

CRediT authorship contribution statement

Yao-Chuan Chang: Conceptualization, Methodology, Formal analysis, Software, Investigation, Data curation, Visualization, Writing - original draft. **Marina Cracchiolo:** Conceptualization, Methodology, Formal analysis, Software, Data curation, Visualization, Writing - original draft. **Umair Ahmed:** Conceptualization, Investigation, Data curation, Validation. **Ibrahim Mughrabi:** Conceptualization, Methodology, Investigation, Data curation. **Arielle Gabalski:** Investigation, Validation. **Anna Daytz:** Investigation, Validation. **Loren Rieth:** Writing - original draft, Resources. **Lance Becker:** Writing - review & editing. **Timir Datta-Chaudhuri:** Resources, Writing - review & editing. **Yousef Al-Abed:** Supervision. **Theodoros P. Zanos:** Methodology, Resources, Visualization, Supervision, Writing - review & editing. **Stavros Zanos:** Conceptualization, Methodology, Funding acquisition, Resources, Supervision, Project administration, Writing - review & editing.

Declaration of competing interest

SZ and YCC have a pending patent application with United Therapeutics Corporation that includes aspects of the research presented in this paper. The other authors declare no conflict of interest.

Acknowledgments

The authors acknowledge Todd Levy, Jacquelyn Tomaio, Khaled Qanud, Naveen Jayaprakash, Adam Abbas, Kevin Tracey, and Thomas Coleman for helpful suggestions and discussion during the study.

Appendix A. Supplementary data

Supplementary data to this article can be found online at https://doi.org/10.1016/j.brs.2020.09.002.

References

[2] Ben-Menachem E. Vagus-nerve stimulation for the treatment of epilepsy. Lancet Neurol 2002;1(8):477–82.
[3] Sackeim HA, Rush AJ, George MS, Marangell LB, Husain MM, Nahas Z, et al. Vagus nerve stimulation (VNS) for treatment-resistant depression: efficacy, side effects, and predictors of outcome. Neuropsychopharmacology. official publication of the American College of Neuropsychopharmacology 2001;25(5):713–28.
[4] Merrill CA, Jonsson MA, Minthon L, Ejnell H, CsS H, Blennow K, et al. Vagus nerve stimulation in patients with Alzheimer's disease: additional follow-up results of a pilot study through 1 year. J Clin Psychiatr 2006;67(8):1171–8.
[5] George MS, Ward Jr HE, Ninan PT, Pollack M, Nahas Z, Anderson B, et al. A pilot study of vagus nerve stimulation (VNS) for treatment-resistant anxiety disorders. Brain stimulation 2008;1(2):112–21.
[6] Chakravarthy K, Chaudhry H, Williams K, Christo PJ. Review of the uses of vagal nerve stimulation in chronic pain management. Curr Pain Headache Rep 2015;19(12):54.
[7] Tyler R, Cacace A, Stocking C, Tarver B, Engineer N, Martin J, et al. Vagus nerve stimulation paired with tones for the treatment of tinnitus: a prospective randomized double-blind controlled pilot study in humans. Sci Rep 2017;7(1):11960.
[8] Koopman FA, Chavan SS, Miljko S, Grazio S, Sokolovic S, Schuurman PR, et al. Vagus nerve stimulation inhibits cytokine production and attenuates disease severity in rheumatoid arthritis. Proc Natl Acad Sci USA 2016;113(29):8284–9.
[9] De Ferrari GM, Stolen C, Tuinenburg AE, Wright DJ, Brugada J, Butter C, et al. Long-term vagal stimulation for heart failure: eighteen month results from

the NEural Cardiac TherApy foR Heart Failure (NECTAR-HF) trial. Int J Cardiol 2017;244:229–34.
[10] Meyers EE, Kronemberger A, Lira V, Rahmouni K, Stauss HM. Contrasting effects of afferent and efferent vagal nerve stimulation on insulin secretion and blood glucose regulation. Physiological reports 2016;4(4).
[11] Pardo JV, Sheikh SA, Kuskowski MA, Surerus-Johnson C, Hagen MC, Lee JT, et al. Weight loss during chronic, cervical vagus nerve stimulation in depressed patients with obesity: an observation. Int J Obes 2007;31(11):1756–9.
[12] Ntiloudi D, Qanud K, Tomaio J-N, Giannakoulas G, Al-Abed Y, Zanos S. Pulmonary arterial hypertension: the case for a bioelectronic treatment. Bioelectronic Medicine 2019;5(1):20.
[13] Yoshida K, Saku K, Kamada K, Abe K, Tanaka-Ishikawa M, Tohyama T, et al. Electrical vagal nerve stimulation ameliorates pulmonary vascular remodeling and improves survival in rats with severe pulmonary arterial hypertension. JACC (J Am Coll Cardiol): Basic to Translational Science. 2018;3(5):657–71.
[14] Bao M, Zhou J, Luan GM. Treatment of drug-resistant epilepsy with vagus nerve stimulation – review of 45 cases. Chinese Med J 2011;124(24):4184–8.
[15] Yoo PB, Lubock NB, Hincapie JG, Ruble SB, Hamann JJ, Grill WM. High-resolution measurement of electrically-evoked vagus nerve activity in the anesthetized dog. J Neural Eng 2013;10(2):026003.
[16] Olofsson PS, Levine YA, Caravaca A, Chavan SS, Pavlov VA, Faltys M, et al. Single-pulse and unidirectional electrical activation of the cervical vagus nerve reduces tumor necrosis factor in endotoxemia. Bioelectronic Medicine 2015;2(1):37–42.
[17] Sundman E, Olofsson PS. Neural control of the immune system. Adv Physiol Educ 2014;38(2):135–9.
[18] Gold MR, Van Veldhuisen DJ, Hauptman PJ, Borggrefe M, Kubo SH, Lieberman RA, et al. Vagus nerve stimulation for the treatment of heart failure: the INOVATE-HF trial. J Am Coll Cardiol 2016;68(2):149–58.
[19] Musselman ED, Pelot NA, Grill WM. Empirically based guidelines for selecting vagus nerve stimulation parameters in epilepsy and heart failure. Cold Spring Harbor perspectives in medicine 2019;9(7).
[20] He S, Teagle HFB, Buchman CA. The electrically evoked compound action potential: from laboratory to clinic. Front Neurosci 2017;11:339.
[21] Parker J L, Shariati N H, Karantonis D M. Electrically evoked compound action potential recording in peripheral nerves. Bioelectronics in medicine 2018;1:71–83.
[22] Rozman J, Peclin P, Ribaric S, Godec M, Burja J. Publisher Correction: an improved method of crafting a multi-electrode spiral cuff for the selective stimulation of peripheral nerves. Sci Rep 2018;8(1):17265.
[23] Geddes LA, Roeder R. Criteria for the selection of materials for implanted electrodes. Ann Biomed Eng 2003;31(7):879–90.
[24] Yoo PB, Liu H, Hincapie JG, Ruble SB, Hamann JJ, Grill WM. Modulation of heart rate by temporally patterned vagus nerve stimulation in the anesthetized dog. Physiological reports 2016;4(2).
[25] Negi S, Bhandari R, Rieth L, Solzbacher F. In vitro comparison of sputtered iridium oxide and platinum-coated neural implantable microelectrode arrays. Biomed Mater 2010;5(1):15007.
[26] Negi S, Bhandari R, Rieth L, Van Wagenen R, Solzbacher F. Neural electrode degradation from continuous electrical stimulation: comparison of sputtered and activated iridium oxide. J Neurosci Methods 2010;186(1):8–17.
[27] Levy TJ, Ahmed U, Tsaava T, Chang YC, Lorraine PJ, Tomaio JN, et al. An impedance matching algorithm for common-mode interference removal in vagus nerve recordings. J Neurosci Methods 2019;330:108467.
[28] Extraction of evoked compound nerve action potentials from vagus nerve recordings. In: Chang Y, Ahmed U, Tomaio JN, Rieth L, Datta-Chaudhuri T, Zanos S, editors. Annu Int Conf IEEE Eng Med Biol Soc. EMBC; 2019. p. 6278–81. DOI: 10.1109/EMBC.2019.8857185.
[29] Mollet L, Raedt R, Delbeke J, El Tahry R, Grimonprez A, Dauwe I, et al. Electrophysiological responses from vagus nerve stimulation in rats. Int J Neural Syst 2013;23(6):1350027.
[30] BEaRJ Tibshirani. An introduction to the bootstrap. Chapman &Hall CRC; 1993.
[31] Chang RB, Strochlic DE, Williams EK, Umans BD, Liberles SD. Vagal sensory neuron subtypes that differentially control breathing. Cell 2015;161(3):622–33.
[32] Judd CM, McClelland GH, Ryan CS. Data analysis : a model comparison approach to regression, anova, and beyond. 2017.
[33] Yao G, Kang L, Li J, Long Y, Wei H, Ferreira CA, et al. Effective weight control via an implanted self-powered vagus nerve stimulation device. Nat Commun 2018;9(1):5349.
[34] Val-Laillet D, Biraben A, Randuineau G, Malbert CH. Chronic vagus nerve stimulation decreased weight gain, food consumption and sweet craving in adult obese minipigs. Appetite 2010;55(2):245–52.
[35] Lee B, Koripalli MK, Jia Y, Acosta J, Sendi MSE, Choi Y, et al. An implantable peripheral nerve recording and stimulation system for experiments on freely moving animal subjects. Sci Rep 2018;8(1):6115.
[36] Somann JP, Albors GO, Neihouser KV, Lu KH, Liu Z, Ward MP, et al. Chronic cuffing of cervical vagus nerve inhibits efferent fiber integrity in rat model. J Neural Eng 2018;15(3):036018.
[37] Qing KY, Wasilczuk KM, Ward MP, Phillips EH, Vlachos PP, Goergen CJ, et al. B fibers are the best predictors of cardiac activity during Vagus nerve stimulation. Bioelectronic Medicine 2018;4(1):5.
[38] McAllen RM, Shafton AD, Bratton BO, Trevaks D, Furness JB. Calibration of thresholds for functional engagement of vagal A, B and C fiber groups in vivo. Bioelectronics in medicine 2018;1(1):21–7.
[39] Agostoni E, Chinnock JE, De Daly MB, Murray JG. Functional and histological studies of the vagus nerve and its branches to the heart, lungs and abdominal viscera in the cat. J Physiol 1957;135(1):182–205.
[40] Lundy DS, Casiano RR, Landy HJ, Gallo J, Gallo B, Ramsey RE. Effects of vagal nerve stimulation on laryngeal function. J Voice : official journal of the Voice Foundation 1993;7(4):359–64.
[41] Vespa S, Stumpp L, Bouckaert C, Delbeke J, Smets H, Cury J, et al. Vagus nerve stimulation-induced laryngeal motor evoked potentials: a possible biomarker of effective nerve activation. Front Neurosci 2019;13:880.
[43] Ahmed U, Chang YC, Cracchiolo M, Lopez MF, Tomaio JN, Datta-Chaudhuri T, et al. Anodal block permits directional vagus nerve stimulation. Sci Rep 2020;10(1):9221.
[44] Hays SA, Rennaker RL, Kilgard MP. Targeting plasticity with vagus nerve stimulation to treat neurological disease. Prog Brain Res 2013;207:275–99.
[45] Boon P, Raedt R, de Herdt V, Wyckhuys T, Vonck K. Electrical stimulation for the treatment of epilepsy. Neurotherapeutics : the journal of the American Society for Experimental NeuroTherapeutics 2009;6(2):218–27.
[46] Castoro MA, Yoo PB, Hincapie JG, Hamann JJ, Ruble SB, Wolf PD, et al. Excitation properties of the right cervical vagus nerve in adult dogs. Exp Neurol 2011;227(1):62–8.
[47] Rajendran PS, Challis RC, Fowlkes CC, Hanna P, Tompkins JD, Jordan MC, et al. Identification of peripheral neural circuits that regulate heart rate using optogenetic and viral vector strategies. Nat Commun 2019;10(1):1944.
[48] Garamendi-Ruiz I, Gomez-Esteban JC. Cardiovascular autonomic effects of vagus nerve stimulation. Clin Auton Res : official journal of the Clinical Autonomic Research Society 2019;29(2):183–94.
[49] Coote JH. Myths and realities of the cardiac vagus. J Physiol 2013;591(17):4073–85.
[50] Gordan R, Gwathmey JK, Xie LH. Autonomic and endocrine control of cardiovascular function. World J Cardiol 2015;7(4):204–14.
[51] Stauss HM. Differential hemodynamic and respiratory responses to right and left cervical vagal nerve stimulation in rats. Physiological reports 2017;5(7).
[52] Jones JF, Wang Y, Jordan D. Activity of C fibre cardiac vagal efferents in anaesthetized cats and rats. J Physiol 1998;507(Pt 3):869–80.
[53] Wang Y, Jones JF, Jeggo RD, de Burgh Daly M, Jordan D, Ramage AG. Effect of pulmonary C-fibre afferent stimulation on cardiac vagal neurones in the nucleus ambiguus in anaesthetized cats. J Physiol 2000;526(Pt 1):157–65.
[54] Bozler E, Burch BH. Role of the vagus in the control of respiration. Am J Physiol 1951;166(2):255–61.
[55] Carr MJ, Undem BJ. Bronchopulmonary afferent nerves. Respirology 2003;8(3):291–301.
[56] Paintal AS. Vagal sensory receptors and their reflex effects. Physiol Rev 1973;53(1):159–227.
[57] Hayashi F, Coles SK, McCrimmon DR. Respiratory neurons mediating the Breuer-Hering reflex prolongation of expiration in rat. J Neurosci : the official journal of the Society for Neuroscience 1996;16(20):6526–36.
[58] Lee LY, Pisarri TE. Afferent properties and reflex functions of bronchopulmonary C-fibers. Respir Physiol 2001;125(1–2):47–65.
[59] Blair EA, Erlanger J. A comparison OF the characteristics OF axons through their individual electrical responses. American Journal of Physiology-Legacy Content 1933;106(3):524–64.
[60] Merrill DR, Bikson M, Jefferys JG. Electrical stimulation of excitable tissue: design of efficacious and safe protocols. J Neurosci Methods 2005;141(2):171–98.
[61] Premchand RK, Sharma K, Mittal S, Monteiro R, Dixit S, Libbus I, et al. Autonomic regulation therapy via left or right cervical vagus nerve stimulation in patients with chronic heart failure: results of the ANTHEM-HF trial. J Card Fail 2014;20(11):808–16.
[62] Aristovich K, Donegà M, Fjordbakk C, Tarotin I, Chapman C, Viscasillas J, et al. Complete optimisation and in-vivo validation of the spatially selective multielectrode array for vagus nerve neuromodulation2019.
[63] Jiao J, Harreby KR, Sevcencu C, Jensen W. Optimal vagus nerve stimulation frequency for suppression of spike-and-wave seizures in rats. Artif Organs 2016;40(6):E120–7.
[64] Gierthmuehlen M, Stieglitz T, Zentner J, Plachta DT. Haemodynamic responses to selective vagal nerve stimulation under enalapril medication in rats. PloS One 2016;11(1):e0147045.
[65] Toader E, Cividjian A, Quintin L. Isoflurane suppresses central cardiac parasympathetic activity in rats: a pilot study. Minerva Anestesiol 2011;77(2):142–6.
[66] Brichant JF, Gunst SJ, Warner DO, Rehder K. Halothane, enflurane, and isoflurane depress the peripheral vagal motor pathway in isolated canine tracheal smooth muscle. Anesthesiology 1991;74(2):325–32.
[67] Skovsted P, Sapthavichaikul S. The effects of isoflurane on arterial pressure, pulse rate, autonomic nervous activity, and barostatic reflexes. Can Anaesth Soc J 1977;24(3):304–14.
[68] Dardai E, Heavner JE. Respiratory and cardiovascular effects of halothane, isoflurane and enflurane delivered via a Jackson-Rees breathing system in temperature controlled and uncontrolled rats. Methods Find Exp Clin Pharmacol 1987;9(11):717–20.

[69] Ardell JL, Nier H, Hammer M, Southerland EM, Ardell CL, Beaumont E, et al. Defining the neural fulcrum for chronic vagus nerve stimulation: implications for integrated cardiac control. J Physiol 2017;595(22):6887–903.
[70] Settell ML, Pelot NA, Knudsen BE, Dingle AM, McConico AL, Nicolai EN, et al. Functional vagotopy in the cervical vagus nerve of the domestic pig: implications for the study of vagus nerve stimulation. J Neural Eng 2020;17(2):026022.
[71] Stakenborg N, Gomez-Pinilla PJ, Verlinden TJM, Wolthuis AM, D'Hoore A, Farre R, et al. Comparison between the cervical and abdominal vagus nerves in mice, pigs, and humans. Neuro Gastroenterol Motil : the official journal of the European Gastrointestinal Motility Society 2020:e13889.
[72] Parent A, Carpenter MB. Carpenter's human neuroanatomy. Baltimore: Williams & Wilkins; 1996. Available from: http://books.google.com/books?id=IJ5pAAAAMAAJ.
[73] Heesch C. Reflexes that control cardiovascular function. Am J Physiol 2000;277:S234–43.
[74] Johnson RL, Wilson CG. A review of vagus nerve stimulation as a therapeutic intervention. J Inflamm Res 2018;11:203–13.
[75] Ben-Menachem E. Vagus nerve stimulation, side effects, and long-term safety. J Clin Neurophysiol: official publication of the American Electroencephalographic Society 2001;18(5):415–8.
[76] Nasi-Er BG, Wenhui Z, HuaXin S, Xianhui Z, Yaodong L, Yanmei L, et al. Vagus nerve stimulation reduces ventricular arrhythmias and increases ventricular electrical stability. Pacing Clin Electrophysiol : PACE (Pacing Clin Electrophysiol) 2019;42(2):247–56.
[77] Zanos S. Closed-loop neuromodulation in physiological and translational research. Cold Spring Harbor perspectives in medicine 2019;9(11).